MDPI

Article

Research on Performance Evaluation Method of Rice Thresher Based on Neural Network

Qiang Da [1,2], Dexin Li [1,*], Xiaolei Zhang [3], Weiling Guo [2], Dongyu He [2], Yanfei Huang [2,*] and Gengchao He [4]

1 Department of Mechanical and Precision Instrument Engineering, Xi'an University of Technology, Xi'an 710048, China
2 National Key Laboratory for Remanufacturing, Army Academy of Armored Forces, Beijing 100072, China
3 College of Engineering, Anhui Agricultural University, Hefei 230000, China
4 School of Materials Science and Engineering, Xi'an University of Technology, Xi'an 710048, China
* Correspondence: lidexin@xaut.edu.cn (D.L.); huangyanfei123@126.com (Y.H.)

Abstract: Because the threshing device of a combine harvester determines the harvesting level and threshing separation performance of a combine harvester, the analysis and study of the threshing device of a combine harvester is key to improving its performance. Based on the threshing device of a half-feed combine harvester, the simulation model of a discrete element threshing device is established in this paper. With the threshing drum rotation speed, feed volume, and concave sieve vibration frequency as the variable factors, the BP neural network model and linear regression equation model established for the loss rate and impurity content for two kinds of threshing performance indicators, respectively, and through the discrete element threshing performance test, two kinds of methods of threshing performance prediction are analyzed. The results show that the neural network and linear regression can be used for the threshing performance indicators, however, the BP neural network prediction effect has a better prediction precision, better reliability, and the trained neural network can be used in the general case of the threshing performance indicators. This provides a new idea for improving the threshing performance of a combine harvester.

Keywords: neural network; rice thresher; threshing performance; prediction

1. Introduction

As the thorough analysis of the threshing process of a combine harvester reveals the cause of incomplete threshing during rice harvest, such as a lack of cleanliness, it is evident that the analysis of a combine harvester's threshing device is necessary to improve the threshing performance—which is key to measuring the combine harvester's threshed rate, loss rate, breakage rate, and impurity rate [1,2].

Current research on the effect of device structure on threshing performance is mainly focused on the continuous improvement and optimization of the structure of the threshing device, so as to improve its threshing performance [3–6]. Abdeen et al. [7] took the threshing machine as their research object and adopted the orthogonal test to analyze the influence relationship between variables such as the drum rotation speed and feed volume and threshing efficiency, power consumption and productivity, and optimize the test variables. Wang et al. [8] improved the design and experimental study of the cutting table and threshing device, and improved the working performance of the whole machine. Teng et al. [9] designed a screw drum segmental threshing system and conducted an optimized test analysis to obtain the optimal combination of the structure and influencing factor parameters. The research results reduced the breakage rate and impurity rate of the screw-drum threshing device. Qian et al. [10] designed flexible threshing teeth and established the dynamic model of the impact friction between the flexible threshing teeth and grain in the threshing process, which verified the reliability and rationality of the flexible teeth and thus reduced the breakage rate of rice.

Research on the factors influencing threshing performance is mainly focused on analyzing and optimizing the parameters of the influencing factors, and provides the basis for improving the threshing performance [11–14]. Miu et al. [15] established the motion equation based on the nonlinear motion between the threshing drum and concave sieve of grain, and studied the motion law of grain in the threshing space of an axial threshing device, providing the basis for the optimization of the threshing device. LOOH et al. [16] designed a self-walking combine harvester according to terrain changes, studied and analyzed its parameters such as concave sieve clearance under different threshing function parameters, conducted three-factor and five-level test analysis with the threshing rate as an indicator, and obtained optimal structural parameters such as the response surface diagram and concave sieve clearance. Zhang et al. [17] studied the performance of the combine harvester under different threshing working parameters, such as the drum rotation speed and threshing clearance, and designed a three-factor quadratic regression center combination test with loss rate as response to obtain the optimal parameter combination of drum rotation speed and threshing clearance.

There have also been many studies on the prediction of threshing performance indicators [18–20]. Gundoshmian et al. [21] and others used a three-layer neural network structure to study the threshing drum rotation speed, concave sieve clearance, fan speed, and other factors affecting the performance of the combine harvester, and established a neural network model to simulate and optimize the traditional combine harvester threshing and separation process which could accurately predict the threshing performance under different conditions of main indicators—namely grain breakage and threshing loss. Li et al. [22] established a neural network model of the loss rate and the parameters of the cleaning system, tested the cleaning performance results of each group under different working conditions, and predicted the loss rate under several conditions. The results show that the prediction results of the model can meet the experimental requirements.

Based on the fluence threshing performance, its influence factors are relatively complex, the neural network model and the linear regression model can be used to predict threshing performance indicators, and as a result, this paper established the BP neural network prediction model and equation of linear regression prediction model to predict the threshing performance indicators, respectively, the comparative analysis and the prediction results.

2. Threshing Performance of Simulation Analysis

The threshing device is the core device of the combine harvester. The movement of the internal mixture is relatively complicated during the working process, and the rice grains and straw are subjected to more forces. It is difficult to simulate the movement process by using the traditional simulation method. Therefore, based on the discrete element theory, EDEM is used to simulate the movement of the mixture in the threshing device and research the movement law of rice and the mixture, which is of great value and theoretical significance to improving the threshing performance.

2.1. Threshing Device of Simulation Model

Based on an arch-toothed threshing device, the discrete element simulation model of a threshing device was established. Figure 1 shows that the arch0toothed threshing device is mainly composed of a threshing drum, concave sieve, shell and other parts. In EDEM, in order to reduce the simulation calculation time, the arch toothed threshing device is simplified to some extent without affecting the simulation results, as follows:

1. Ignore the parts that are irrelevant to the calculation and analysis, such as the bearing block, connectors, bearings, and support frames;
2. Arch teeth are simplified, the welding seam ignored, and use a small size structure, such as bolt gasket;
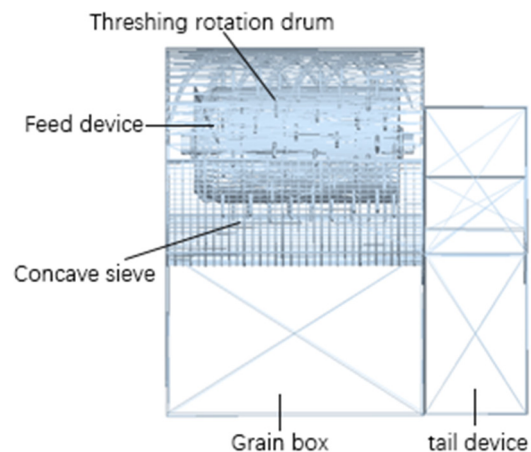3. Remove the fillets and chamfering at both ends of the threshing drum.

Figure 1. Simplified threshing device model.

However, the size of the main moving parts is consistent with the actual size of the combine harvester, and the threshing device is modeled and assembled by SolidWorks 2019.

As shown in Figure 1, the grain is transported to the threshing device through the feed device. Under the action of continuous rotation and the percussion of the threshing rotation drum, the grain and straw are separated through impact, kneading, and other threshing processes. Most of the grains fall into the grain box through the concave sieve, and the short straw and a few grains are discharged out of the tail device.

Herein, rice is used as an example, and the rice mixture in the threshing device includes grain kernels, short straw, and glume shell. Other debris refers to grain leaves, dust, weeds, and other light debris, which accounts for a very small percentage of the total weight. The rice mixture moving in the threshing device was mainly grains and short straw, accounting for nearly 99% of the total weight of the mixture. In order to simplify the types of grain models and improve the simulation efficiency, in this paper, only the effects of rice grains and short straw were considered—whilst the effects of debris, etc., were not considered.

Combined with the actual motion state of the rice mixture, it can be seen from Figure 2 that the centrifugal force generated by the threshing drum in the discrete element simulation model of the threshing device makes the total particle mixture move forward along the circular shape formed by the inner wall of the top cover of the threshing device and the inner contour of the concave plate screen.
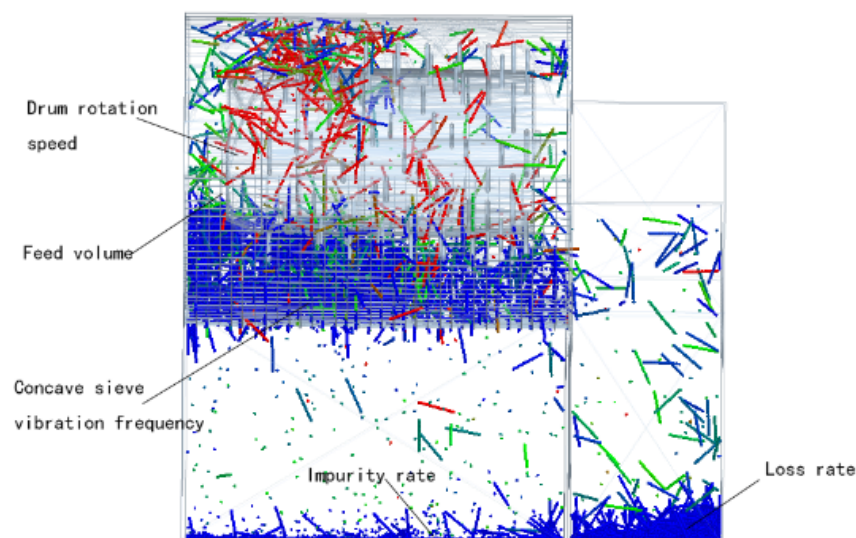

Figure 2. Working process of threshing device model.

After the simulation, a very small part of the short straw fell into the grain box from a hole in the concave plate sieve, and a very small part of the grain was discharged along with the tail device.

The grain movement was consistent with the actual threshing device. Therefore, the effectiveness of the simulation model can be established.

As shown in Figure 3 and Table 1, according to the actual three-dimensional shape and size of the rice, the grain and short stem are established in EDEM. The grain kernels are roughly ellipsoids, the long axis of the rice kernels is 7.6 mm, and the cross-section along the length direction is a circle, whilst the diameter of the circle on the maximum cross-section is 3.5 mm. The short straw is a hollow cylinder with a length of approximately 80 mm; whilst the cross-section is a circle with a diameter of 4 mm.

Grain particle

Short straw particle

Figure 3. Grain and short straw particles.

Table 1. Grain and short straw particles parameters.

	Rice	**Short Straw**
Length (mm)	7.6	80
cross section	circle	cylinder
cross section diameter (mm)	3.5	4.0

2.2. Threshing Device Simulation Parameters of Setting

In order to more accurately establish the models of the grain kernels, short straw, and threshing device, the mechanical property parameters and contact coefficients of grains such as grain should be input before the simulation begins. The experimental data results of the references are cited [23], and the mechanical properties and contact coefficients of grains are summarized in Tables 2 and 3.

Table 2. Threshing device and grain mechanical parameters.

	E **(Pa)**	ν	ρ **(kg/m**^{3}**)**
grain	1×10^7	0.3	1350
short straw	2.6×10^7	0.4	100
threshing device	7×10^{10}	0.3	7800

Note: E: modulus of elasticity; ν: Poisson's ratio; ρ: density.

Table 3. Contact parameters in EDEM.

	Recovery Coefficient	**Static Friction Coefficient**
grain—grain	0.2	1.0
grain—short straw	0.2	0.8
grain—threshing device	0.5	0.58
short straw—short straw	0.2	0.9
short straw—threshing device	0.2	0.8

Note: all value of rolling friction coefficient is 0.01.

Due to the limitation of experimental conditions and simulation time, a particle factory was established in the geometry module of EDEM to simultaneously produce rice grain particles and short straw particles. The total weight of the rice grain and short straw was 1 kg; the grain generation time was 3 s; the feed volume of threshing device was set to 0.66 kg/s; the particle feed rate was set to 0.33 m/s; the number of rice grains was 2928; and the number of short straws was 1326.

The simulation time step is determined by Rayleigh wave method. If the simulation time step is too large, the particles will disappear and interfere with the threshing device, while if the time step is too small, the simulation time will be increased. Therefore, the Rayleigh time step is set to 10%; total simulation time was 5 s; the output time interval was 0.01 s; and the Hertz–Mindlin contact model was selected.

2.3. Threshing Performance of Simulation Results

In this paper, the loss rate and impurity rate were selected to measure the threshing performance of the threshing device [24].

The loss of grains refers to the grains entailed in the mixture discharged from the end of the threshing device, and the loss rate refers to the percentage of the loss of grain mass in the total input grain mass. Its Equation (1) is as follows:

$$a = \frac{m_1}{M_1} \times 100\% \tag{1}$$

where a denotes the loss rate (%); m_1 represents the weight of lost grains (kg); and M_1 is the total weight of total grains (kg).

The impurity rate refers to the percentage of impurity mass to the total mass of the mixture from the bottom of the threshing device. Its Equation (2) is as follows:

$$b = \frac{m_2}{M_2} \times 100\% \tag{2}$$

where b denotes the loss rate (%); m_2 represents the weight of lost grains (kg); and M_2 is total weight of total grains (kg).

A simulation analysis of the threshing performance of the drum rotation speed was carried out in EDEM. The drum rotation speed starts from 400 r/min, and a simulation test was conducted at an interval of 100 r/min. The feed volume was 1.0 kg/s; the vibration frequency of the concave sieve was set at 6 Hz [25]; and the results of the loss rate and impurity rate of the threshing drum at 8 speeds are shown in Table 4 and Figure 4.

Table 4. Different drum rotation speeds on loss and impurity rate.

Drum Rotation Speed (r/min)	400	500	600	700	800	900	1000	1100
loss rate *(%)*	6.56	5.43	5.29	5.16	5.53	5.91	6.39	6.76
impurity rate *(%)*	8.09	8.26	9.12	9.43	9.72	10.67	11.44	11.96

Note: feed volume 1.0 kg/s; the vibration frequency is 6 Hz.

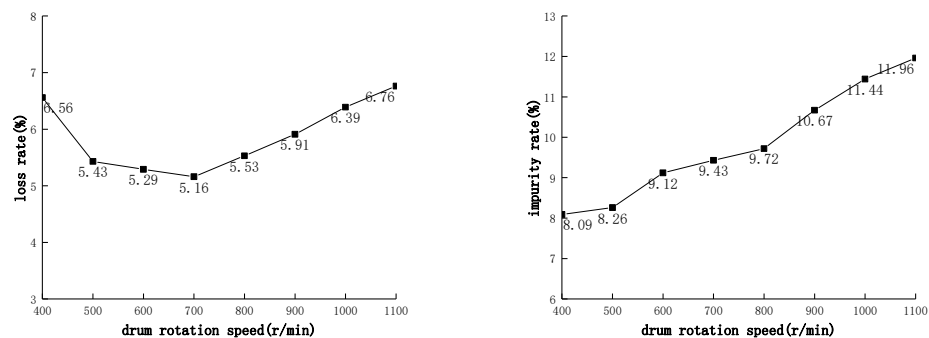**Figure 4.** Effect of drum rotation speeds on loss and impurity rate.

It can be seen from Table 4 and Figure 4 that when the drum speed is lower than 700 r/min, the drum speed increases successively and the loss rate decreases gradually. On the contrary, the loss rate increases gradually when the drum speed is 700 r/min—and the minimum loss rate is 5.16%. When the drum speed is between 600 r /min and 800 r/min,

the loss rate changes little. When the drum speed is more than 900 r/min, the loss rate increases obviously.

Similarly, when the drum rotation speed is 800 r/min, the vibration frequency is 6 Hz, and the feed volume is 0.4~1.6 kg/s; a simulation test was carried out at an interval of 0.2 kg/s. The results of the loss rate and impurity rate of the threshing device under seven feed volumes are shown in Table 5 and Figure 5.

Table 5. Different feed volume on the loss and impurity rate.

Feed Volume (kg/s)	0.4	0.6	0.8	1.0	1.2	1.4	1.6
loss rate (%)	4.23	4.37	4.82	5.05	5.19	6.01	6.15
impurity rate (%)	7.96	8.18	9.27	9.62	9.89	10.81	11.65

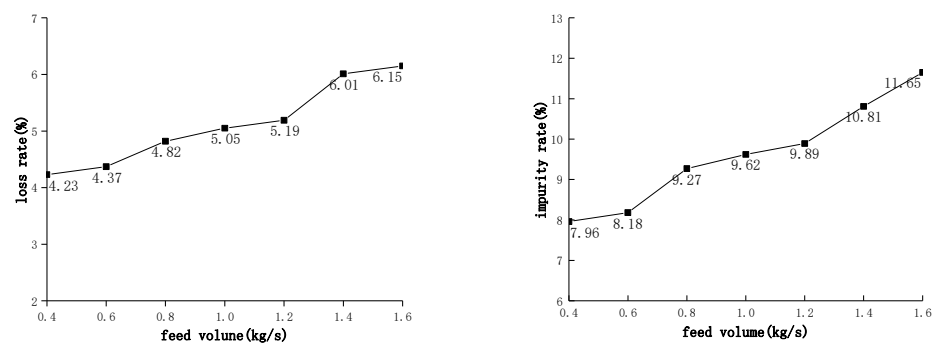Note: the drum rotation speed is 800 r/min; the vibration frequency is 6 Hz.

Figure 5. Effect of different feed volume on loss and impurity rate.

As can be seen from Table 5 and Figure 5, when the feed volume increased gradually, the loss rate and impurity rate also increased gradually, but when the feed volume was between 0.8 and 1.2 kg/s, the increase range of the loss rate and impurity rate was relatively smoothly.

Similarly, when the drum rotation speed is 800 r/min, the feed volume is 1.0 kg/s, and the vibration frequency is 3~9 Hz, a simulation test is carried out in an interval of 1 Hz. The results of the loss rate and impurity rate of the threshing drum under seven vibration frequencies are shown in Table 6 and Figure 6.

Table 6. Different vibration frequencies on the loss and impurity rate.

Vibration Frequency (Hz)	3	4	5	6	7	8	9
loss rate (%)	6.22	5.91	5.33	5.12	5.02	4.75	4.37
impurity rate (%)	8.93	9.11	9.97	9.82	9.48	8.88	8.44

Note: the drum rotation speed is 800 r/min; the feed volume is 1.0 kg/s.

As can be seen from Table 6 and Figure 6, when the vibration frequency increases in turn, the loss rate decreases continuously, but when the vibration frequency is 3~5 Hz, the impurity rate increases; when the vibration frequency is 5~9 Hz, the impurity rate gradually decreases.

To sum up, the variation rules of the drum rotation speed, the feed volume, and vibration frequency on threshing performance indicators can be obtained.
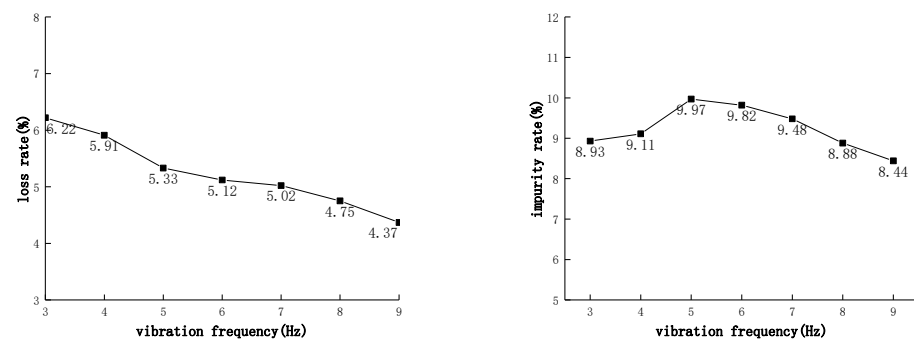
Figure 6. Effect of different vibration frequencies on loss and impurity rate.

3. BP Neural Network and Linear Regression Model

Based on the single factor test, the results of the threshing performance indicators change were analyzed. Taking the drum rotation speed, feed volume, and vibration frequency of the concave sieve as variables, the corresponding simulation experiment was designed and the loss rate and the impurity rate of the threshing performance indicators were obtained. The BP neural network model and linear regression model were established according to the experimental results.

3.1. Selection of Influencing Factor Level

According to the analysis of single factor test results, the influence law of each influencing factor on the threshing performance is known.

Therefore, the value range of each test factor level was selected based on the single-factor test, as shown in Table 7.

Table 7. Level table of experimental factors.

Level	Factors		
	Drum Rotation Speed (r/min)	Feed Volume (kg/s)	Vibration Frequency (Hz)
1	600	0.8	5
2	700	1.0	6
3	800	1.2	7

3.2. BP Neural Network Model of Establishment and Results

Because of the uncertainty of the threshing condition and the complexity of the influencing factors of threshing device, the relationship of the threshing performance is nonlinear. The prediction of the threshing performance of the combine harvester under different influencing parameters provides ideas and methods for the optimization of the threshing device.

The prediction of the threshing performance is regarded as a nonlinear problem jointly acted by a variety of influencing factors by using the strong nonlinear and generalization ability of the BP neural network so as to achieve the prediction of the threshing performance test indicators under different parameters and reduce the repetition times of the threshing performance test [26].

According to Table 7, a three-layer neural network structure with two hidden layers is established, as shown in Figure 7, and a three-factor and three-level comprehensive experiment was designed to generate 27 groups of sample data—as shown in Table 8.
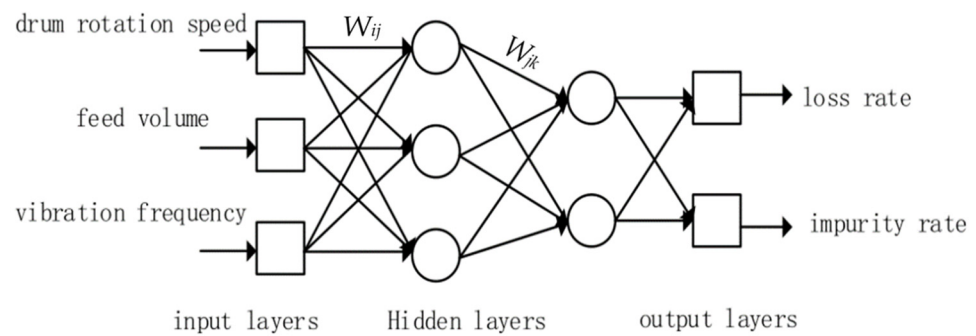
Figure 7. Neural network structure diagram of threshing performance.

Table 8. Twenty-seven groups of relevant data generated from the comprehensive test.

Drum Rotation Speed (r/min)	Feed Volume (kg/s)	Vibration Frequency (Hz)	Loss Rate (%)	Impurity Rate (%)
600	0.8	5	4.68	8.07
600	0.8	6	4.58	7.93
600	0.8	7	4.37	7.58
600	1.0	5	4.85	8.35
600	1.0	6	4.78	7.95
600	1.0	7	4.51	7.72
600	1.2	5	4.99	8.65
600	1.2	6	4.88	8.22
600	1.2	7	4.71	8
700	0.8	5	4.61	8.46
700	0.8	6	4.47	8.19
700	0.8	7	4.3	7.84
700	1.0	5	4.68	8.8
700	1.0	6	4.54	8.39
700	1.0	7	4.41	7.98
700	1.2	5	4.98	8.96
700	1.2	6	4.78	8.61
700	1.2	7	4.64	8.14
800	0.8	5	4.51	8.72
800	0.8	6	4.33	8.31
800	0.8	7	4.27	7.92
800	1.0	5	4.61	8.85
800	1.0	6	4.54	8.52
800	1.0	7	4.44	8.12
800	1.2	5	4.75	9.06
800	1.2	6	4.64	8.67
800	1.2	7	4.37	8.24

As can be seen from Figure 7, W_{ij} and W_{jk} are the value of the weight. In the process of designing the threshing performance, the BP neural network structure, the number of neurons in each layer, the activation function, the number of hidden layers in the network, the number of input and output layers, and other key parameters should be fully considered.

1. Considering the drum rotation speed, feed volume, and the vibration frequency, loss rate, impurity rate, the principle of BP neural network nonlinear modeling, the training sample dimension, and the input nodes as the input layers for three factors, namely drum rotation speed, feed volume, and vibration frequency, whilst the output layers are the loss rate and impurity rate;

2. When the number of hidden layers is large, the reliability of the error signal propagating back from the output layer to input layer decreases. In addition, the increase in the number of hidden layers will reduce the learning efficiency and increase the time

cost of network training. As for the number of hidden layers, it is generally better to have as few as possible under the condition of meeting the requirements dealt with it in this paper is relatively simple. According to this principle, a three-layer neural network with two hidden layers was selected for training and learning;

3. The number of neurons will indirectly affect the performance of the neural network. Neurons at each layer of the neural network structure are connected to all neurons at the next layer through corresponding characteristic function transformation, while there is no connection between the neurons at each layer of the neural network and no direct corresponding connection with the outside world.

4. The threshing performance prediction model is trained by Levenberg–Marquardt method, the training function is trained, the maximum training times is 100, the training accuracy is 0, the maximum number of failures is 6, the minimum gradient is 1×10^{-10}, the initial value of Mu is 0.001, and the maximum value of Mu is 1×10^{10}. The hidden layer is divided into two layers, in which the transfer function purelin in the first layer, logsig, transfer function of the second layer, show an interval of 10 and set an error target of 10^{-3}, whilst the rest of the settings of the default value are adopted in the network training process, and the parameters such as the coefficient of the network structure, network parameters, calculation process, and these parameters which are related to each other are adopted. As such, the end value is obtained through the study of different combinations of these parameters and step-by-step debugging.

According to the BP neural network and experimental indicators system and Kolmogorov theorem [27], the input layer has three nodes, so the number of neurons in the hidden layer 2R + 1 is seven, and R is the number of nodes in the input layer. Equation (3) can also be used to calculate the number of hidden layer nodes.

$$n_1 = \sqrt{n + k} + c \tag{3}$$

where n denotes the number of nodes in the output layer, k represents the number of nodes in the input layer, n_1 is the number of nodes in the hidden layer, and c is a constant ranging from approximately 1 to 10.

As the experimental data units of the BP neural network input layer are inconsistent, their values differ greatly, which finally leads to the slow convergence of the neural network results and longer training time of sample set. All input data are normalized to prevent the phenomenon that the information with a small value in dataset is annihilated by the information with large value, as shown in Equation (4).

$$y = \frac{(x - x_{min})}{x_{max} - x_{min}} \tag{4}$$

where x denotes the original data, x_{max} and x_{min} represent the maximum value and minimum value of the original data training set, respectively, and y is the normalized data.

The principle of the neural network using the objective function is to minimize the sum of squares of the error of the output variables of parameters to be estimated on training samples, as shown in Equation (5):

$$\min Q = \frac{1}{2} \sum_{j=1}^{m} \sum_{i=1}^{n} \left[y_{ij} - f_j\left(\hat{B}, x_{it}\right) \right]^2 = \frac{1}{2} \sum_{j=1}^{m} \sum_{i=1}^{n} \left[f_j(B, x_{it}) - f_j\left(\hat{B}, x_{it}\right) \right]^2 \tag{5}$$

where x_{it} denotes the value of the i sample on the t input variable; y_{ij} represents the value of the i sample on the j output variable; f_j is the input/output function of the neural network; B is the unestimated parameter where $B = [\beta_1, \beta_2 ... \beta_n]$. $n = (q - m) * r$, q is the number of input variables, m is the number of output variables, r is the number of intermediate neurons, and $\hat{B}$ is the parameter to be estimated.

$\hat{B} = \left[\hat{\beta}_1, \hat{\beta}_2 \cdots \hat{\beta}_n\right], \hat{B}$ satisfies

$$-\frac{\partial Q}{\partial \beta_s} = \sum_{j=1}^{p} \sum_{i=1}^{q} \frac{\partial \beta_j\left(\hat{B}, x_{ij}\right)}{\partial \overset{\wedge}{\beta_s}} \left[f_j(B, x_{it}) + u_{ij} - f_j\left(\hat{B}, x_{it}\right)\right] = 0 \tag{6}$$

where $s = 1, 2, 3 \cdots n$; p is number of training samples; and u_{ij} is random error term,

When $p + q \gg n$, $\hat{B}$ is the unbiased estimation. For this paper, $q = 3$, $r = 7$, $m = 2$, $n = 35$, $p = 18$, that is the sample size must be greater than 18, and the total number of tests in this paper is 27 groups, which meets this condition.

The 27 groups of experiments were divided into two parts, with 23 groups as the training set and 4 groups as the test set. When the error reaches the set stop condition or the number of iterations ends, the training is stopped, as shown in Figures 8 and 9.
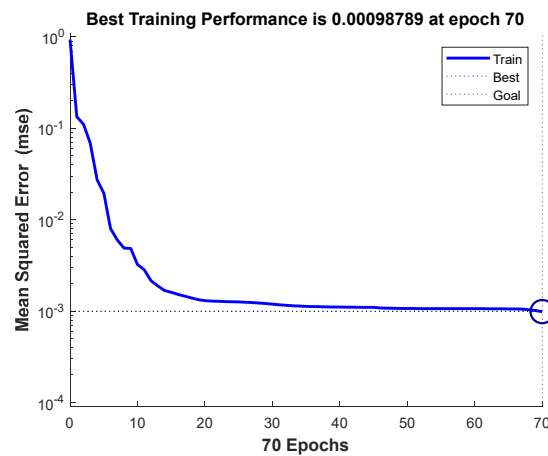

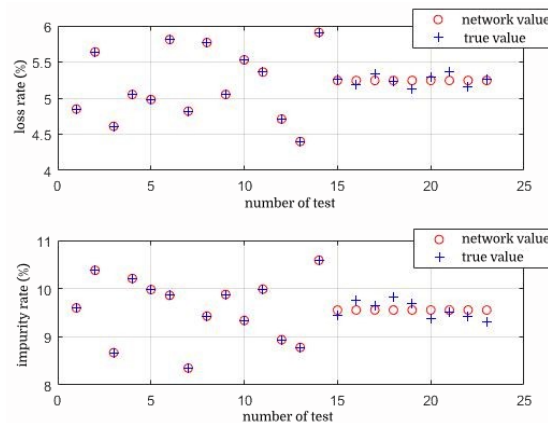**Figure 8.** Curve of root mean square error and number of iterations.

Figure 9. BP neural network sample training results.

It can be seen from Figure 8 that the root mean square error of training samples decreases with the increase in iterations. After 70 iterations, the best training result is 0.00098789. When the error reached the set stop condition or the number of iterations ended, the training was stopped.

As shown in Figure 9, the sample's predicted value of the neural network training is quite close to the actual value, and the error accuracy also satisfies the set requirements.

3.3. Linear Regression Model of Establishment and Results

The mathematical model between the loss rate and impurity rate of the test indicators and the influencing factors can be obtained through the fitting of the secondary center

combined test, which can be used to predict the test indicators. The level coding table of the design factors is designed as shown in Table 9.

Table 9. Level coding table of design factors.

Z_i	X_1 (r/min)	X_2 (kg/s)	X_3 (Hz)
asterisk arm $+\gamma$	800	1.2	7
level +1	759.45	1.119	6.594
level 0	700	1.0	6
level −1	640.55	0.881	5.406
asterisk arm $-\gamma$	600	0.8	5

The factor level coding table designed according to the selected factor level is shown in Table 10. Reference [28] calculated the total number of tests as 23 groups.

Table 10. Center rotation combination test and results.

Serial	Z_1	Z_2	Z_3	Y_1 (%)	Y_2 (%)
1	1	1	1	4.85	9.60
2	1	1	−1	5.60	10.38
3	1	−1	1	4.47	8.67
4	1	−1	−1	5.16	10.21
5	−1	1	1	4.99	9.98
6	−1	1	−1	5.84	9.86
7	−1	−1	1	4.75	8.35
8	−1	−1	−1	5.43	9.43
9	1.682	0	0	5.05	9.88
10	−1.682	0	0	5.53	9.34
11	0	1.682	0	5.36	9.99
12	0	−1.682	0	4.71	8.94
13	0	0	1.682	4.40	8.78
14	0	0	−1.682	5.91	10.59
15	0	0	0	5.26	9.44
16	0	0	0	5.19	9.76
17	0	0	0	5.33	9.65
18	0	0	0	5.23	9.83
19	0	0	0	5.12	9.69
20	0	0	0	5.29	9.38
21	0	0	0	5.36	9.51
22	0	0	0	5.16	9.43
23	0	0	0	5.26	9.31

According to the results of the threshing performance indicators, the loss rate Y_1 and impurity rate Y_2 are shown in Table 10.

The optimal solution of the influencing factors was obtained by regression fitting, and then the threshing performance indicators were predicted. A linear regression equation is generally adopted, as shown in Equation (7):

$$Y = a + \sum_{j=1}^{m} b_j x_j + \sum_{k<j}^{k=1} b_{kj} x_k x_j + \sum_{j=1}^{m} b_{jj} x_{jj}^2, k = 1, 2, \cdots, m-1 \tag{7}$$

where, a, b_j, b_{kj}, and b_{jj} denote the regression coefficient; m represents the factor; x_k, x_j are the variable factors; and Y is the test indicator.

A polynomial fitting method was used to obtain the regression equations Y_1 and Y_2 between the loss rate and impurity rate of the test indicators, and the rotational speed of drum, feed volume, and vibration frequency of concave sieve for Y_1 and Y_2 are as shown in Table 11.

Table 11. The parameters value of equation Y_1 and Y_2.

	a	b_1	b_2	b_3	b_{12}	b_{23}	b_{13}	b_{11}	b_{22}	b_{33}
Y_1	542	−0.25	0.29	−0.68	0.26	0.19	−0.09	0.05	−0.20	−0.08
Y_2	9.56	0.27	0.66	−0.77	−0.40	−0.47	0.82	0.03	−0.11	0.11

The parameter values in equations Y_1 and Y_2 are as shown in Table 11.

4. Threshing Performance Indicators of Prediction and Comparison

In this paper, four groups of experimental simulation data in Table 8 were randomly selected and variable factors were introduced into the neural network model and linear regression model, respectively, to obtain the prediction results of threshing performance indicators, which were compared and analyzed with the experimental data. The experimental data and results are shown in Table 12. Parameter combination and threshing performance of four groups of different influencing factors.

Table 12. Select four groups of experiment data and results.

Drum Rotation Speed (r/min)	Feed Volume (kg/s)	Vibration Frequency (Hz)	Loss Rate (%)	Impurity Rate (%)
600 (1)	1.0	6	5.29	9.12
700 (2)	0.8	5	5.12	9.76
700 (3)	1.2	5	5.96	10.01
800 (4)	0.8	7	4.55	8.47

4.1. Prediction Results of BP Neural Network

When the neural network training reached the setting error range, we took the experiment data in Table 12 as test set detection data to verify the trained BP neural network model, as shown in Figure 10.
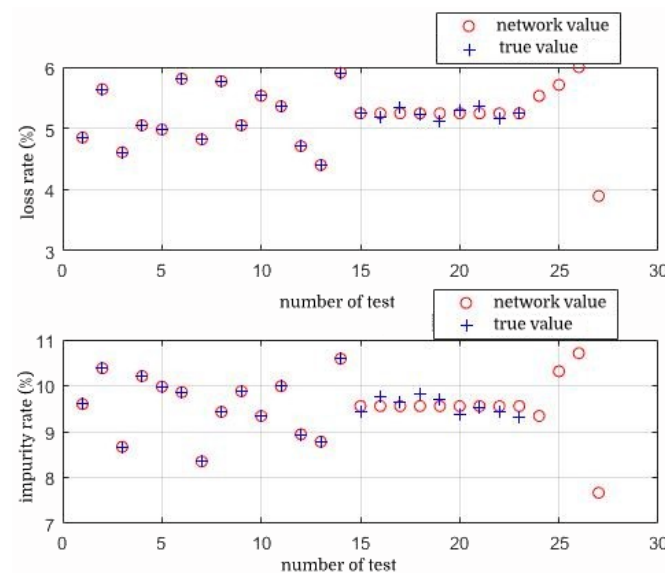

Figure 10. Neural network training with predictive data added.

After adding four groups of data, the prediction model of the BP neural network is shown in Table 13.

Table 13. Neural network prediction of threshing performance.

Drum Rotation Speed (r/min)	Feed Volume (kg/s)	Vibration Frequency (Hz)	Loss Rate (%)	Impurity Rate (%)
600 (1)	1.0	6	5.53	9.34
700 (2)	0.8	5	5.71	10.31
700 (3)	1.2	5	6.00	10.71
800 (4)	0.8	7	3.89	7.67

4.2. Prediction Results of Linear Regression

The established linear regression model was used to predict and verify the threshing performance indicators. The combination of the influencing factor parameters in Table 13 was substituted into Table 11, and the results are shown in Table 14.

Table 14. Linear regression model prediction of threshing performance.

Drum Rotation Speed (r/min)	Feed Volume (kg/s)	Vibration Frequency (Hz)	Loss Rate (%)	Impurity Rate (%)
600 (1)	1.0	6	5.72	9.32
700 (2)	0.8	5	5.44	10.49
700 (3)	1.2	5	6.20	10.17
800 (4)	0.8	7	3.99	7.54

4.3. Analysis and Comparison

The results are compared with those of the neural network prediction model and the linear regression prediction model. Additionally, the results are shown in Tables 15 and 16.

Table 15. Comparison of prediction errors of loss rate network model.

Group Number	1	2	3	4
measured values	5.29	5.62	5.96	4.55
linear regression predicted value	5.72	5.44	6.20	3.99
absolute error	−0.43	0.18	−0.24	0.56
error rate (%)	−8.13	3.20	−4.03	12.3
neural network predicted value	5.53	5.71	6.00	4.39
absolute error	−0.24	−0.09	−0.04	0.16
error rate (%)	4.54	1.60	0.067	0.35

Table 16. Comparison of prediction errors of impurity rate network model.

Group Number	1	2	3	4
measured values	9.12	9.76	10.51	8.47
linear regression predicted value	9.32	10.49	10.17	7.54
absolute error	−0.20	−0.73	0.34	0.93
error rate (%)	2.19	−7.48	3.24	10.98
neural network predicted value	9.24	10.31	10.71	7.67
absolute error	0.12	−0.55	−0.2	0.8
error rate (%)	1.32	5.64	−1.90	9.45

Table 15 shows that for the loss rate, the minimum absolute error of the linear regression model is 0.18%, the maximum absolute error is 0.56%, the minimum error rate of the linear regression model is 3.20%; and the maximum error rate is 12.3%. The minimum absolute error of the neural network nonlinear prediction model is −0.04, the maximum absolute error is −0.24, the minimum error rate of the neural network nonlinear prediction model is 0.067%, and the maximum error rate is 4.54%.

Table 16 shows that, for the impurity rate, the minimum absolute error of the linear regression model is 0.20%, the maximum absolute error is 0.93%, the minimum error rate of linear regression model is 2.19%, and the maximum error rate is 10.98%. The minimum absolute error of the neural network nonlinear prediction model is −0.12, the maximum absolute error is 0.8, the minimum error rate of neural network nonlinear prediction model is 1.32%, and the maximum error rate is 9.45%.

In conclusion, it can be seen that both the BP neural network model and the linear regression model have a good prediction effect on threshing performance. Through analysis and comparison, the prediction accuracy of the BP neural network was determined to be better than that of the linear regression model include absolute error and error rate.

5. Conclusions

Threshing performance indicators are an important standard to measure and the prediction for optimization, and are important to measure the combine harvester's level of performance. This article selected the drum rotation speed, feed volume, and concave sieve vibration frequency as the factors influencing the loss rate and impurity rate for the threshing performance indicators and established the BP neural network model and the linear regression equation model to predict the threshing performance indicators. Through the comparative analysis and the prediction results, it was concluded that the BP neural network and linear regression can be used for threshing performance prediction, but the BP neural network prediction accuracy has a small error rate compared with the linear regression model of absolute error, and provides a new method of thinking in order to optimize the combine harvester threshing performance. The trained neural network can be used for general threshing performance prediction and can reduce the number of experiments—saving time and cost.

Author Contributions: Conceptualization, Q.D. and D.L.; methodology, Q.D.; software, Q.D and G.H.; validation, X.Z., formal analysis, D.L., X.Z., and G.H.; investigation, Q.D.; resources, Q.D.; data curation, X.Z.; writing—original draft preparation, Q.D.; writing—review and editing, W.G.; visualization, Y.H.; supervision, D.H.; project administration, D.L.; funding acquisition D.L. All authors have read and agreed to the published version of the manuscript.

Institutional Review Board Statement: Not applicable.

Inform Consent Statement: Not applicable.

Data Availability Statement: Not applicable.

Conflicts of Interest: The authors declare no conflict to interest.

References

1. Hasan, M.K.; Ali, M.R.; Saha, C.K.; Alam, M.M.; Haque, M.E. Combine Harvester: Impact on paddy production in Bangladesh. *J. Bangladesh Agric. Univ.* **2019**, *17*, 583–591. [CrossRef]
2. Tang, Z.; Zhang, H.; Zhou, Y. Unbalanced vibration identification of tangential threshing cylinder induced by rice threshing process. *Shock Vib.* **2018**, *2018*, 4708730. [CrossRef]
3. Cao, K.; Li, Z.; Gu, Y.; Zhang, L.; Chen, L. The control design of transverse interconnected electronic control air suspension based on seeker optimization algorithm. *Proc. Inst. Mech. Eng. Part D J. Automob. Eng.* **2021**, *235*, 2200–2211. [CrossRef]
4. Singh, P.; Chaudhary, H. Optimum discrete balancing of the threshing drum using Jaya algorithm. *Mech. Based Des. Struct. Mach.* **2019**, *12*, 100–114. [CrossRef]
5. Choe, J.S.; Inoue, E.; Hashiguchi, K. Development of design theory on the tooth arrangement and the threshing drum for a large-sized and high-speed head-feeding combine. *Agric. Multidiscip.* **2000**, *44*, 377–384. [CrossRef]
6. Yuan, J.; Li, H.; Qi, X.; Hu, T.; Bai, M.; Wang, Y. Optimization of airflow cylinder sieve for threshed rice separation using CFD-DEM. *Eng. Appl. Comput. Fluid Mech.* **2020**, *14*, 871–881. [CrossRef]

7. Abdeen, M.A.; Salem, A.E.; Zhang, G. Longitudinal Axial Flow Rice Thresher Performance Optimization Using the Taguchi Technique. *Agriculture* **2021**, *11*, 88. [CrossRef]

8. Wang, Q.; Bai, Z.; Li, Z.; Xie, D.; Chen, L.; Wang, H. Straw/Spring Teeth Interaction Analysis of Baler Picker in Smart Agriculture via an ADAMS-DEM Coupled Simulation Method. *Machines* **2021**, *9*, 296. [CrossRef]

9. Teng, Y.; Chen, Y.; Jin, C.; Yin, X. Design and test on the type of spiral cylinder-segmented concave threshing system. In Proceedings of the 2019 ASABE Annual International Meeting, Boston, MA, USA, 7–10 July 2019; American Society of Agricultural and Biological Engineers: Boston, MA, USA, 2019; p. 1.

10. Qian, Z.; Jin, C.; Zhang, D. Multiple frictional impact dynamics of threshing process between flexible tooth and grain kernel. *Comput. Electron. Agric.* **2017**, *141*, 276–285. [CrossRef]

11. Singh, K.P.; Pardeshi, I.L.; Kumar, M.; Srinivas, K.; Srivastva, A.K. Optimisation of machine parameters of a pedal-operated paddy thresher using RSM. *Agric. Eng.* **2008**, *100*, 591–600. [CrossRef]

12. Lin, Z.; Zhao, X.; Zhao, Z.; Wang, S. Process Optimization for Preparation of Metallic Powders by Exploding Foil with Pulsed Laser. *Mater. Rep.* **2022**, *36*, 21080257-6.

13. Rao KN, V.; Balguri, P.K.; Govardhan, D.; Vamsi, C.K.; Sravani, M. Design and material optimization of an Orion re-entry aeroshell for higher structural performance. *Mater. Today Proc.* **2022**, *62*, 2730–2738. [CrossRef]

14. Wang, Q.; Mao, H.; Li, Q. Modelling and simulation of the grain threshing process based on the discrete element method. *Comput. Electron. Agric.* **2020**, *178*, 105790. [CrossRef]

15. Miu, P.I.; Kutzbach, H.D. Mathematical model of material kinematics in an axial threshing unit. *Comput. Electron. Agric.* **2007**, *58*, 93–99. [CrossRef]

16. Looh, G.A.; Xie, F.; Mangeh, F.C., III; Wang, X.; Wang, X. Performance Assessment of a Self-propelled Paddy Grain Thresher under Different Threshing Functional Parameters. *Appl. Eng. Agric.* **2020**, *36*, 141–149. [CrossRef]

17. Zhang, D.; Yi, S.; Zhang, J.; Bao, Y. Establishment of millet threshing and separating model and optimization of harvester parameters. *Alex. Eng. J.* **2022**, *61*, 11251–11265. [CrossRef]

18. Singh, K.P.; Mishra, H.N.; Saha, S. Optimization of Machine Parameters of Finger Millet Thresher-Cum-Pearler. *Agric. Eng.* **2010**, *41*, 60–67.

19. Powar, R.V.; Aware, V.V.; Shahare, P.U. Optimizing operational parameters of finger millet threshing drum using RSM. *Food Sci. Technol.* **2019**, *56*, 3481–3491. [CrossRef] [PubMed]

20. Chaab, R.K.; Karparvarfard, S.H.; Rahmanian-Koushkaki, H.; Mortezaei, A.; Mohammadi, M. Predicting header wheat loss in a combine harvester, a new approach. *J. Saudi Soc. Agric. Sci.* **2020**, *19*, 179–184. [CrossRef]

21. Gundoshmian, T.M.; Ghassemzadeh, H.R.; Abdollahpour, S.; Navid, H. Application of artificial neural network in prediction of the combine harveseter performance. *J. Food Agric. Environ.* **2010**, *8*, 721–724.

22. Li, B.; Li, T.; Jiang, Q.; Huang, H.; Zhang, Z.; Wei, Y.; Sun, B.; Jia, X.; Li, B.; Yin, Y. Prediction of Cleaning Loss of Combine Harvester Based on Neural Network. *Int. J. Pattern Recognit. Artif. Intell.* **2020**, *34*, 2059021. [CrossRef]

23. Liquan, T.; Zhengzhong, Z.; Yongsen, X.; Meiqiao, L.; Rendiao, J. Development and experiment on 4LZ-4.0 type double speed and double action rice combine harvester. *Int. J. Front. Eng. Technol.* **2020**, *2*, 1–15. [CrossRef]

24. Ma, X.; Guo, B.; Li, L. Simulation and experiment study on segregation mechanism of rice from straws under horizontal vibration. *Biosyst. Eng.* **2019**, *186*, 1–13. [CrossRef]

25. Wang, Q.; Zhang, Q.; Zhang, Y.; Zhou, G.; Li, Z.; Chen, L. Lodged Sugarcane/Crop Dividers Interaction: Analysis of Robotic Sugarcane Harvester in Agriculture via a Rigid-Flexible Coupled Simulation Method. *Actuators* **2022**, *11*, 23. [CrossRef]

26. Yu, C.; Zhu, D.; Gao, Y.; Xue, K.; Zhang, S.; Liao, J.; Liu, J. Optimization and experiment of counter-rotating straw returning cultivator based on discrete element method. *J. Adv. Mech. Des. Syst. Manuf.* **2020**, *14*, JAMDSM0097. [CrossRef]

27. Zhang, X. A study on the risk assessment of ship oil spill accidents in the case of small samples. *Ship Eng.* **2009**, *31*, 76–80.

28. Wang, S. The unpredictability of standard back propagation neural networks in classification applications. *Manag. Sci.* **1995**, *41*, 555–559. [CrossRef]